Engineering the Membrane/Electrode Interface to Improve the Performance of Solid-State Supercapacitors

Chun Huang[a*], *Jin Zhang*[b], *Henry J. Snaith*[b] *and Patrick S. Grant*[a]

[a]Department of Materials, University of Oxford, Oxford, OX1 3PH, UK

[b]Clarendon Laboratory, University of Oxford, Oxford, OX1 3PH, UK

E-mail: `ann.huang@materials.ox.ac.uk`

Abstract

This paper investigates the effect of adding a 450 nm layer based on porous TiO_2 at the interface between a 4.5 μm carbon/TiO_2 nanoparticle-based electrode and a polymer electrolyte membrane as a route to improve energy storage performance in solid-state supercapacitors. Electrochemical characterisation showed that adding the interface layer reduced charge transfer resistance, promoted more efficient ion transfer across the interface and significantly improved charge/discharge dynamics in a solid-state supercapacitor, resulting in an increased areal capacitance from 45.3 to 111.1 mF cm^{-2} per electrode at 0.4 mA cm^{-2}.

Keywords: interface engineering; porous TiO_2 particles; solid-state supercapacitor; spray processing; wearable energy storage applications

1 Introduction

Supercapacitors have a quick response (<1 s) for storing and releasing electrical energy through rapid absorption/desorption of electrolyte ions over a high surface area electrode.[1–3] Most commercial supercapacitors use carbon-based electrodes and liquid organic electrolytes such as tetraethylammonium tetrafluoroborate (TEATFB) in propylene carbonate or acetonitrile.[4,5] Solid-state supercapacitors that replace the liquid electrolytes with an ion conducting polymer gel and the separator with an ion-conducting polymer electrolyte membrane do not require rigid packaging to contain the liquid electrolytes. Consequently, solid-state energy storage devices can be thinner, lighter and provide greater design freedom.[6–9] They are thus potentially attractive for applications such as future wearable electronics and conformal energy storage systems.

The main weakness of solid-state supercapacitors is the reduced ion mobility within the electrodes, within the polymer electrolyte membrane itself, and at the electrode/membrane interface,[10] which combine to undermine the key supercapacitor advantage of high power. Major advances have been made in higher ion-conducting solid-state electrolytes such as an ionogel consisting of an ionic liquid confined within a silica host network,[11] an alginate-based gel electrolyte with ionic liquid,[12] a poly(ethylene oxide)(PEO)-1-ethyl-3-methylimidazolium hydrogensulfate ($EMIHSO_4$) electrolyte with SiO_2 and TiO_2 nanofillers,[13] and Keggin structured heteropolyacids/polymer composite electrolytes.[14] Advances have also been made in processing techniques such as ink-jet printing of a silica-based ionogel confined with ionic liquid to increase areal charge storage,[8] *in situ* UV-initiated polymerisation of an extended interface between highly porous electrodes and a polymer gel electrolyte to increase power,[10] and ion soft landing of redox-active molybdenum polyoxometalate (POM) anions at the interface between electrode and ionic liquid electrolyte membrane to increase redox reactivity.[15]

In terms of the electrodes, composite electrodes containing multi-wall carbon nanotubes (MWNTs) and TiO_2 nanoparticles have shown promising performance in supercapacitors. For example, an electrode containing conformal porous TiO_2 coating on carbon nanotubes exhibited a capacitance of 87.5 F g^{-1} at 0.5 A g^{-1} in a 0.5 M H_2SO_4 electrolyte,[16] while a layer-by-layer (LbL) assembled 760 nm thick electrode of sub-8 nm TiO_2 particles and MWNTs exhibited a high capacitance of 262 F g^{-1} at 5 mV s^{-1} in a 0.5 M H_2SO_4 electrolyte.[17] We have previously demonstrated a ∼10 μm thick electrode in a solid-state supercapacitor, based on an interconnected MWNT scaffold decorated with non-porous TiO_2 nanoparticles (N-TiO_2, 20 nm) in which both the MWNTs and N-TiO_2 were coated with a layer of ionomer (monomer of Nafion polymer). The MWNT scaffold provided electrical conduction throughout the electrode, and inhibited excessive agglomeration of the N-TiO_2 nanoparticles, while the ionomer coating provided H^+ ion conduction throughout the electrode. The capacitance increased 2.5 times for the electrode containing both MWNTs and N-TiO_2 nanoparticles (weight ratio 2:1) compared with an electrode containing MWNTs only, because the N-TiO_2 nanoparticles contributed toward a high electrode surface area for ion adsorption (electric double layer capacitance, EDLC) and pseudo-capacitance between the -OH group on the TiO_2 nanoparticles and H^+ ions in the ionomer coating.[18] We have also previously demonstrated the addition of a graphene interface layer between the electrode and current collector to improve electrical conductivity in a solid-state supercapacitor.[19].

Despite these improvements in electrolytes, energy storage materials and electrode fabrication, solid-state supercapacitor performance lags significantly behind liquid electrolyte supercapacitors. Modelling has suggested that it is the interface between the electrode and the polymer electrolyte membrane contributes significant ionic resistance that undermines solid-state supercapacitor performance and the overall rate of charge/discharge.[20–23] Therefore, it can be speculated that engineering of this interface, for example by the addition of an interface layer that improves the physical interaction and ion mobility between the polymer electrolyte membrane and the electrode may help to recover acceptable device performance. In this paper, we investigate the performance of a N-Ti_2/MWNT solid-state supercapacitor, without and with a thin (∼450 nm), porous TiO_2 (P-TiO_2) based interface layer, sprayed directly onto a Nafion polymer electrolyte membrane as shown in Figure 1(a). This interface layer exploits the additional ion pathways provided by the P-TiO_2 to improve ion mobility across the interface with the polymer electrolyte membrane, and we demonstrate significant improvements in the overall charge storage behaviour.

2 Experimental

The detailed experimental methods for synthesising P-TiO_2 single crystals, spray procedure and characterisation methods are described in the Supporting Information (SI). We have reported the atomisation spray processing in detail before.[24] Briefly, two aqueous suspensions for A - the interface layer, and B - the electrode were prepared: (A) P-TiO_2, MWNTs, sodium dodecylbenzenesulfonate (SDBS) and Nafion ionomer in 0.5 M H_2SO_4; and (B) N-TiO_2, MWNTs, SDBS and Nafion ionomer in 0.5 M H_2SO_4, where SDBS was used as a surfactant in both suspensions. Table 1 summarises the composition of the two aqueous suspensions.

During the electrode fabrication, multi-nozzles sprayed consecutively suspensions of the interface materials (suspension A) and then the electrode materials (suspension B) in a continuous process

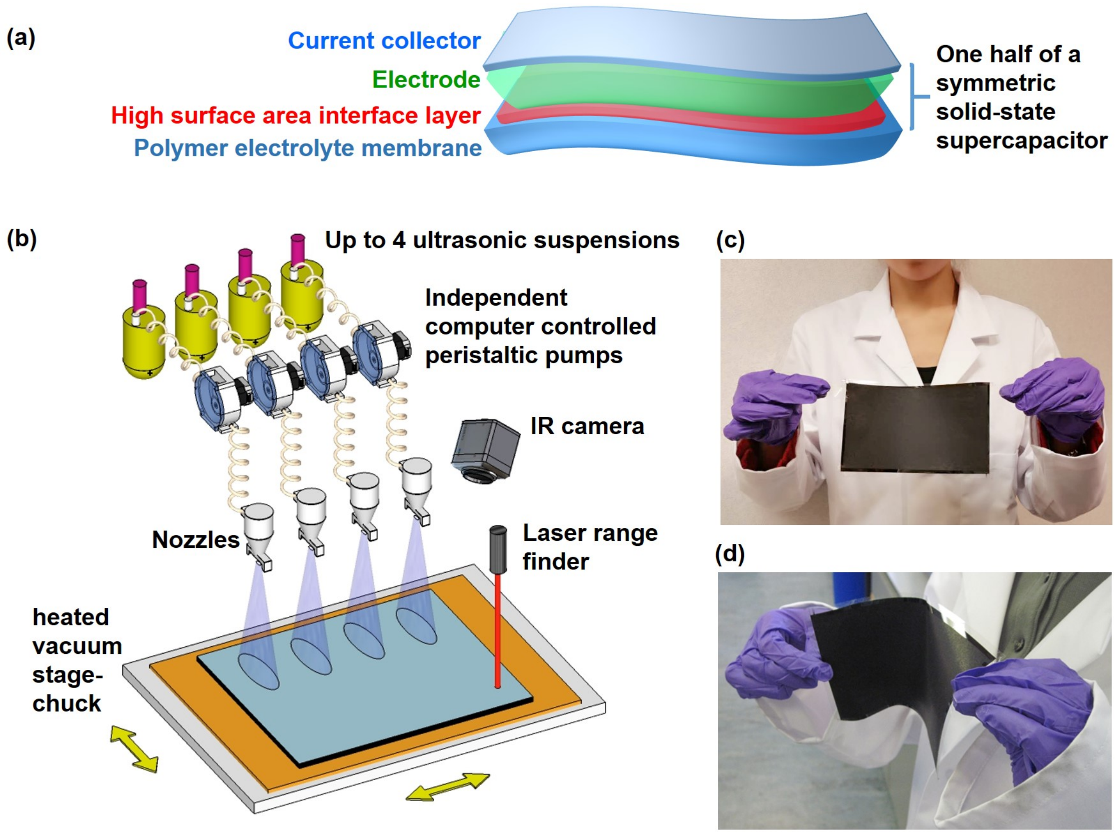

Figure 1: Schematic diagrams of (a) one half of a solid-state supercapacitor with a high surface area interface layer between the electrode and the polymer electrolyte membrane and (b) spray deposition arrangement used to layer-by-layer fabricate the interface layer and the electrode; (c) photo of an as-sprayed 16 cm x 9.5 cm solid-state supercapacitor to show scalability of the spray processing technique; and (d) photo of the same size solid-state supercapacitor to show flexibility.

with no breaks between layers (Figure 1(b)). The suspensions were atomised into fine droplets by compressed air and deposited onto an acid-treated H^+ ion-conducting Nafion membrane, maintained at 100 ^{o}C throughout fabrication on a heated vacuum stage. The nozzles moved in a pre-programmed zig-zag pattern in the X and Y plane to fabricate an electrode up to 20 cm x 20 cm. The fugitive water from the sprayed suspension evaporated continuously on the heated vacuum stage as first the interface layer and then the electrode layer were deposited successively. The membrane with one side covered with the interface layer and the electrode was then flipped and the other side sprayed using the identical procedure, to directly form a solid-state supercapacitor

Sprayed aqueous suspension	**wt%**				
	$P\text{-}TiO_2$	$N\text{-}TiO_2$	MWNT	Nafion ionomer	SDBS
A	55	0	11	33	1
B	0	22	44	33	1

Table 1: The composition of the two types of sprayed aqueous suspension.

Electrode	**wt%**				
	$P\text{-}TiO_2$	$N\text{-}TiO_2$	MWNT	Nafion	SDBS
[$N\text{-}TiO_2$ + MWNT] electrode ([N])	0	22	44	33	1
[$N\text{-}TiO_2$ + MWNT] electrode with a [$P\text{-}TiO_2$ + MWNT] interface layer ([I])	5	20	41	33	1

Table 2: A summary of the composition of the two types of electrode.

with no need for any subsequent re-immersion in liquid electrolytes. The average mass loading of the electrodes was 1.1 mg cm^{-2} ± 3.1%. In the interface layer, the weight ratio of $P\text{-}TiO_2$: MWNT : Nafion ionomer was 5:1:3, while for the rest of the electrode, the weight ratio of $N\text{-}TiO_2$: MWNT : Nafion ionomer was 2:4:3. Figures 1(c) and (d) show a 16 cm x 9.5 cm solid-state supercapacitor with full retention of electrodes on both sides, fabricated by the spray method, indicating scalability of the processing technique and the robustness of the resulting solid-state supercapacitor.

In order to investigate the effect of the interface layer, two types of electrode were sprayed: one without the interface layer (termed [N] electrode), and the other with the interface layer (termed [I] electrode), and their compositions are summarised in Table 2. For both types of electrode, the total thickness was kept at $\sim$5 μm ±2.7%.

The surface morphology of the electrodes was examined by scanning electron microscopy (SEM JEOL 6500F at 10 kV). The electrode materials were examined by high resolution transmission electron microscopy (TEM JEOL 2100F at 200 kV). The porosity of the sprayed layers was evaluated through mercury porosimetry using a Micromeritics AutoPore IV operating at a pressure of 3.5 to 2 x 10^5 kPa. The conductivity of the electrodes without and with the interface layer was measured using a standard four-point probe configuration and a Keithley 220 programmable current source meter. Sprayed electrodes on Si wafers were used to exclude any conductivity contributions from metal current collectors. An indication of the wettability of the H_2SO_4 impregnated Nafion membrane with the two types of TiO_2 was investigated using an IT Concepts Tracker goniometer by measuring the contact angle between the N-TiO_2 and the P-TiO_2 sprayed layers and a drop of 0.5 M H_2SO_4. Both conductivity and wettability measurements were repeated eight times on each electrode to obtain an average.

Solid-state supercapacitors of area 1.13 cm^2 and 1.2 cm diameter were punched from the two-side sprayed polymer electrolyte membrane. Two pieces of stainless steel current collectors (25 μm) were pressed onto the two sides of the solid-state supercapacitor and assembled into a swagelok cell in air. A range of electrochemical testing (cyclic voltammetry (CV), galvanostatic charge/discharge and electrochemical impedance spectroscopy (EIS)) was performed on the solid-state supercapacitor in the swagelok cell using a Reference 600/EIS300 Gamry potentiostat/galvanostat.

3 Results and discussion

3.1 Microstructure and the electrode/membrane interface

Figure 2(a) is a scanning electron microscopy (SEM) image of the sprayed electrode comprising non-porous TiO_2 nanoparticles mixed with MWNTs [N-TiO_2 + MWNT] showing an interconnected MWNT network decorated with the N-TiO_2 nanoparticles. Figure 2(b) is a transmission electron microscopy (TEM) image showing more clearly the TiO_2 decorated MWNTs and that, as intended, both the MWNTs and the N-TiO_2 were coated with the ion-conducting ionomer, essential to facilitate ion transport throughout the electrode.[25] The crystal lattice planes of the N-TiO_2 nanoparticles shown in the high resolution TEM image in Figure 2(c) had a (101) d-spacing of 0.313 nm, conforming to highly crystalline anatase TiO_2.

Figure 2(d) is an SEM image of the laboratory synthesised pristine P-TiO_2 particles of $\sim$180 nm size, showing their porous structure with $\sim$20 nm diameter internal pores that penetrated through the particles. Figure 2(e) is a cross-sectional SEM image of an electrode with the interface layer based on this P-TiO_2 between the Nafion membrane and the rest of the [N-TiO_2 + MWNT] electrode. The interface layer thickness was approximately 450 nm, while the rest of the electrode had a thickness of $\sim$4.5 μm, extending beyond the field of view in Figure 2(e). Figure 2(f) is a magnified cross-sectional SEM image of the interface layer showing P-TiO_2 particles and MWNTs.

To investigate if there was any limited inter-mixing between the interface layer and the rest of the electrode, the cross-section of an electrode in which the mass ratio of TiO_2 : MWNT was 1:1 for both the interface layer and electrode (so that any observed porosity or morphology change was due to differences between the P-TiO_2 and N-TiO_2 only) was investigated in the SEM. Figure S1

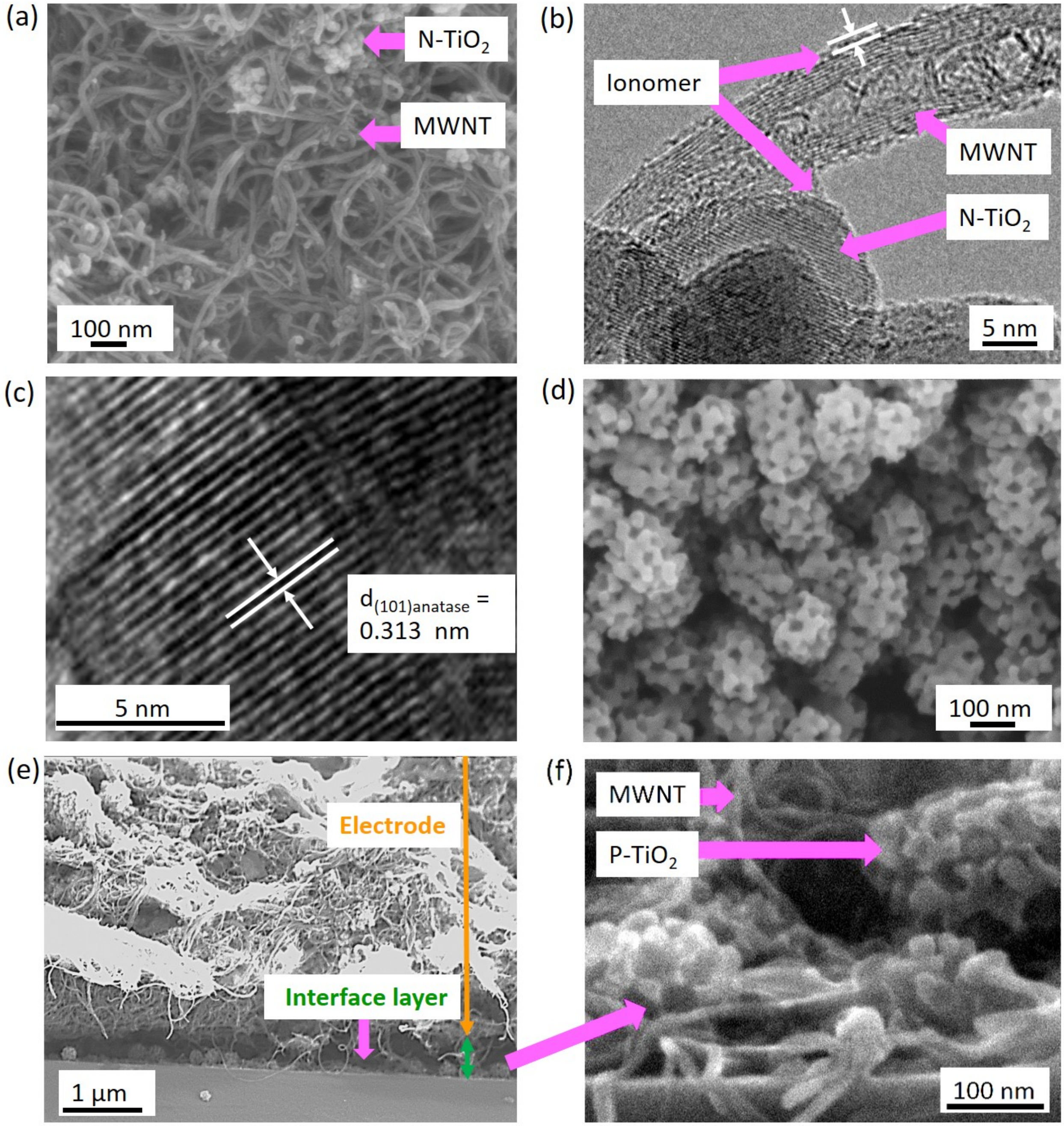

Figure 2: (a) SEM image of a sprayed electrode of MWNT scaffold decorated with non-porous TiO_2 nanoparticles [N-TiO_2 + MWNT]; (b) TEM image of MWNTs decorated with N-TiO_2 nanoparticles in the electrode; (c) high resolution TEM image of magnified N-TiO_2 nanoparticles with crystall lattice planes; (d) SEM image of laboratory synthesised pristine P-TiO_2 particles; (e) cross-sectional SEM image of the electrode with the interface layer between the Nafion membrane and the rest of the electrode; and (f) magnified cross-sectional SEM image of the interface layer.

in the SI shows an SEM image of the region between the interface layer (brightest) and electrode (darkest), confirming higher porosity in the interface layer and some fine-scale inter-mixing in a 250 - 370 nm thickness zone between the interface layer and the electrode.

3.2 Porosity of the electrode and the interface layer

We now study the effect of the two different TiO_2 morphologies on the resulting porosity of each of the sprayed layers, by depositing each separately onto a 10 μm thick Cu foil. Although most mercury infiltration porosimetry measurements are performed on powders,[26] here the porosity of the *sprayed layers* on a Cu foil was measured by mercury porosimetry. The two layers studied were: (i) a mixture of P-TiO_2 and MWNTs (termed [P] layer), and (ii) a mixture of N-TiO_2 and MWNTs (termed [N] layer). For mercury infiltration measurements, neither layer contained any ionomer coating that might block pores and affect the measurements, which was considered acceptable since the purpose of these experiments was to estimate the relative contributions of the different types of TiO_2 to the overall layer porosity, which - on the basis of the earlier SEM images - can be expected to be substantially filled with ionomer in the working electrodes. The sprayed layer thickness was approximately 5 μm and similar to the working electrodes. A 1:1 TiO_2 : MWNT mass ratio was used for both layers, rather than 1:2 used in the working electrodes to show more clearly the relative contribution of the TiO_2 morphology to the layer porosity.

A control test was performed first to confirm that the Cu foil did not contribute to the measurement of porosity. Then, during mercury infiltration of the sprayed layer, hydrostatic pressure was increased progressively to infiltrate the mercury from the upper side of the layer “down” into the layer itself, as a way of mimicking the way ions may infiltrate into the electrode once coated in ionomer, from the polymer electrolyte membrane. Figure 3 shows the mercury intrusion volume as a function of pressure for both the [P] and [N] layers, showing a higher mercury intrusion volume for the [P] layer than the [N] layer at all pressures, by a factor of up to ∼1.75, indicating that the intrinsic higher porosity of the P-TiO_2 particles was preserved into the sprayed layer. The higher porosity of the [P] layer implied a larger fraction of the H^+ ion-conducting ionomer can be incorporated into the layer that in turns enables a greater EDLC.

The average contact angle of H_2SO_4 (present in the polymer electrolyte membrane and in the sprayed suspensions) with the [P] and [N] layers was 48.7^o and 66^o respectively. The lower contact angle for the [P] layer suggested a better wettability with the H^+ containing membrane.[27] Therefore, a P-TiO_2 based layer was chosen to form the first deposited, interface layer between the polymer electrolyte membrane and the N-TiO_2 based layer that formed the bulk of the electrode. The P-TiO_2 based layer was intended to facilitate H^+ ion mobility to and from the acid-treated Nafion membrane (high H^+ concentration) to the rest of the electrode (low H^+ concentration).

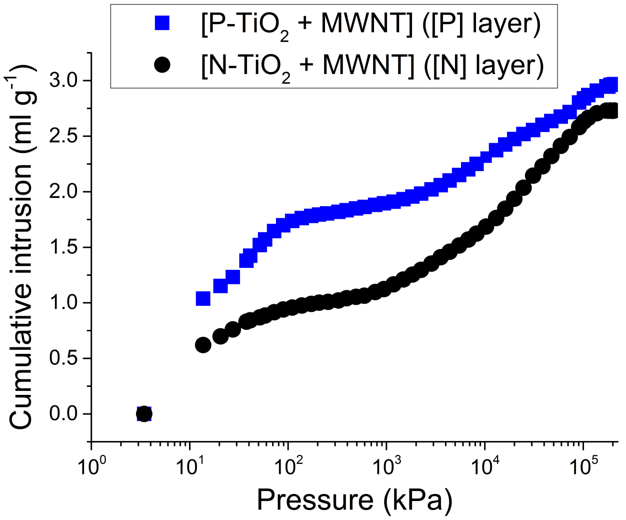

Figure 3: Mercury intrusion volume curves as a function of pressure for the two types of layer: (i) a mixture of P-TiO_2 and MWNTs ([P]); and (ii) a mixture of N-TiO_2 and MWNTs ([N]).

3.3 Ion transport and the effect of the interface layer

We now study the rate of ion transport behaviour in the [N-TiO_2 + MWNT] electrode without the interface layer (electrode [N]) and with the interface layer (electrode [I]) in a solid-state supercapacitor configuration, as shown in the schematic diagram in Figure 1(a). Figure 4(a) shows Nyquist plots without and with the interface layer at 0.01 - 10^5 Hz, where the electrochemical impedance $Z = Z' + jZ''$, and Z' and Z'' are the real and imaginary parts of the impedance.[38] Figure 4(b) shows a zoomed-in region of the Nyquist plots to show more clearly the behaviour at high frequency. There was an excellent fit between the experimental data and model-based simulation data using the equivalent circuit in Figure 4(d).

In the equivalent circuit in Figure 4(d), *ESR* is the equivalent series resistance that includes electrolyte resistance and contact resistance,[28] R_{CT} is the charge transfer resistance of the electrode and the interfacial resistance between the electrode and polymer electrolyte membrane,[29] *CPE* is the constant phase element that describes the capacitance of a porous electrode,[30] and *W* is the Warburg element that describes ion diffusion within a porous electrode.[1,31] The parallel combination of CPE_2 and R_{CT} in the equivalent circuit represents the semi-circle in the high frequency domain in the Nyquist plot, followed by a linear part of the Nyquist plot in the low frequency domain. The two regimes are often connected by a line of almost 45^o slope which is referred to as the Warburg impedance.[32] There are two types of frequency dispersion that deviate a Nyquist plot from an ideal shape of a semi-circle and a vertical line: one is in-pore dispersion that signifies the diminishing penetration depth of an ac signal with frequency; and the other is multiple penetration depths in multiple pore sizes of the electrode.[33] Therefore, two *CPE* elements were used in the equivalent circuit in Figure 4(d), where CPE_1 is responsible for the change in the slope of the

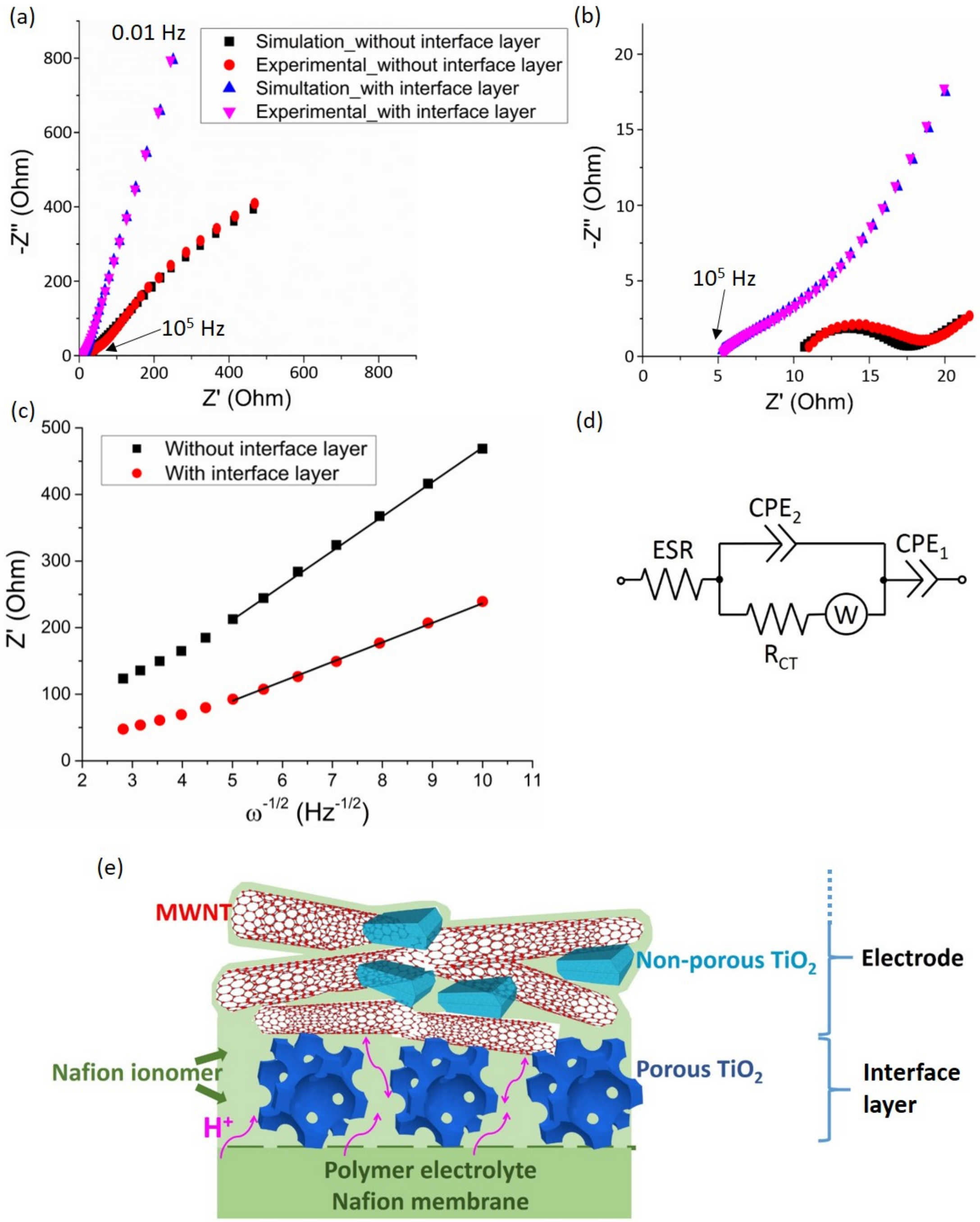

Figure 4: Experimental and simulated Nyquist plots of solid-state supercapacitors before and after adding the interface layer (a) in the 0.01 - 10^5 frequency range; and (b) in the high frequency range only; (c) a plot showing the correlation between real impedance (Z') and frequency$^{-1/2}$ ($\omega^{-1/2}$) of solid-state supercapacitors in the low frequency region using the electrodes without and with the interface layer; (d) the equivalent circuit used to generate the simulation data in the Nyquist plots; and (e) a schematic showing the role of the interface layer in improving ion transport from the polymer electrolyte Nafion membrane to the rest of the electrode (diagram not to scale).

Electrode	**ESR** (Ω**cm**^{2})		**R**$_{CT}$ (Ω**cm**^{2})	
	Experimental	Simulation	Experimental	Simulation
[N-TiO$_2$ + MWNT] electrode ([N])	12.4	12.0	9.6	9.3
[N-TiO$_2$ + MWNT] electrode with a [P-TiO$_2$ + MWNT] interface layer ([I])	5.7	5.5	4.1	4.0

Table 3: A summary of the experimental and simulated data for the resistances shown in the Nyquist plots in Figures 4(a) and (b).

Warburg impedance in the mid-frequency domain and CPE_2 is responsible for the change in the slope of the vertical line in the low frequency region.[32,33]

The *ESR* was estimated from the intercept of the Nyquist plot with the *Z'* axis at high frequency at 12.4 and 5.7 Ωcm^2, before and after adding the interface layer. The estimated *ESR* was higher than the *ESR* of similar electrodes in a liquid electrolyte,[34] but consistent with 8.4-13.6 Ωcm^2 measured for other high-performing solid-state supercapacitors.[35] The lower *ESR* after adding the interface layer was due to the higher wettability of the P-TiO$_2$ with the polymer electrolyte membrane so that the ionomer filled internal pores of the P-TiO$_2$ could act as efficient pathways for ion movement to and from the electrode. R_{CT} was estimated from a best-fit semi-circle to the data at high frequency,[36] and was related to the ease of charge transport, including the ion transport at the interface between the electrode and polymer electrolyte membrane.[36,37] R_{CT} before and after adding the interface layer was estimated at 9.6 and 4.1 Ωcm^2 respectively. The reduced R_{CT} after adding the interface layer in Figure 4(b) suggested improved ion transport at the interface.[32] Table 3 gives the experimental and simulation data for the electrodes before and after adding the interface layer, showing excellent agreement.

The gradient of the “tail” in the middle to low frequency in Figure 4(a) indicated the rate of ion diffusion from the Nafion membrane into the electrode.[37,38] The electrode with the interface layer exhibited a steeper gradient than the electrode without, indicating faster ion diffusion.[39] To quantify the rate of ion diffusion, Figure 4(c) shows the real impedance Z' as a function of the reciprocal square root of frequency $\omega^{-1/2}$ in the low frequency range of 0.01-0.126 Hz.[40] The best-fit gradients to the data indicate the diffusion rates, and the diffusion rate changed with frequency as ions were redistributed.[29] In this case, linear responses were observed in the lowest frequency range of 0.01-0.04 Hz, as shown in Figure 4(c), where the gradient of the best-fit straight lines is the Warburg ion diffusion resistance,[41] that was estimated at 51.3 $\Omega s^{-1/2}$ and 29.4 $\Omega s^{-1/2}$ for the electrodes before and after adding the interface layer.

The *ESR*, R_{CT} and Warburg ion diffusion resistance data taken as a whole indicated consistently that adding the interface layer improved the dynamics of ion transfer. This arose because (i) the P-TiO_2 in the interface layer had relatively good wetting with the polymer electrolyte membrane, and (ii) the P-TiO_2 provided higher interfacial porosity to promote ion movement, both from/to the polymer electrolyte membrane into/out of the rest of the electrolyte during charge/discharge, as shown schematically in Figure 4(e).

As described above, the thickness ratio between the interface layer and the electrode was approximately 1:10 in order to use the P-TiO_2 conservatively. However, to understand what performance might be achieved in an electrode comprising entirely [P-TiO_2 + MWNT], a 5 μm thick electrode (termed [P] electrode) was studied. Figure 5(a) shows the Nyquist plots from the [N], [I] and [P] electrodes ([N-TiO_2 + MWNT] only, [N-TiO_2 + MWNT] electrode with a [P-TiO_2 + MWNT] interface layer, and [P-TiO_2 + MWNT] only respectively). For the [P] electrode, the semi-circle at high frequency gave the lowest R_{CT} ~1.4 Ωcm^2 due to its greater porosity, as shown in the earlier infiltration experiments. Despite using only ~10% of the [P-TiO$_2$ + MWNTs] in thickness, the gradient of the "tail" in the middle to low frequency for the [I] electrode was similar to that of the [P] electrode, and much steeper than that of the [N] electrode. Thus, at a thickness ratio of only 1:10 for the interface layer, placing the P-TiO$_2$ at the polymer electrolyte membrane/electrode interface only, dramatically improved ion diffusion and ion transport, approaching that of the [P] electrode.

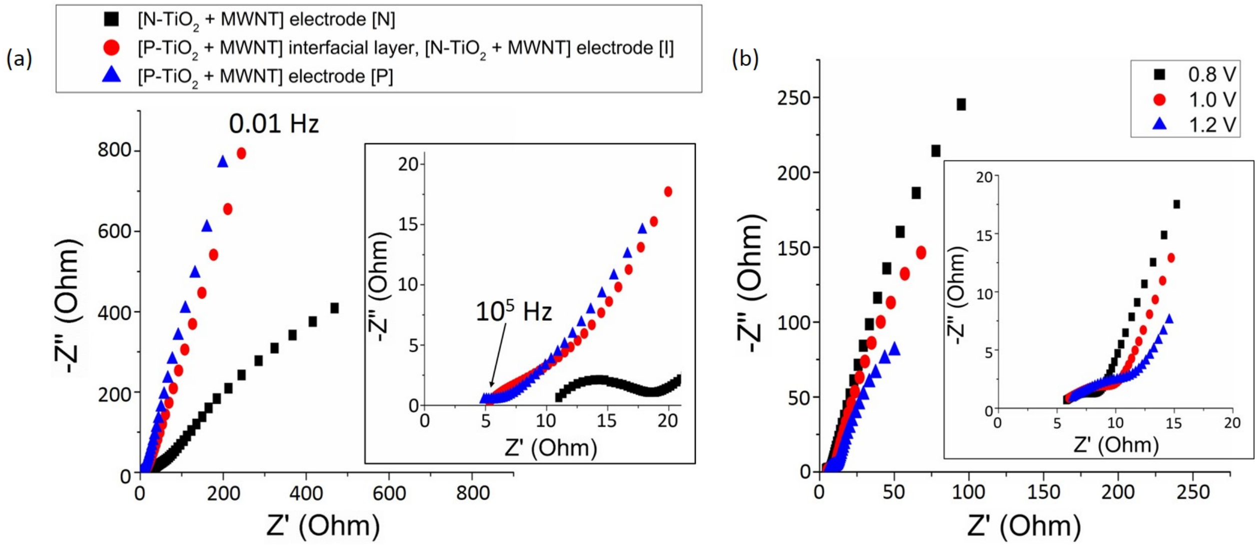

Figure 5: (a) Nyquist plots of the solid-state supercapacitors using [N], [I] and [P] electrodes and otherwise identical; and (b) Nyquist plots of the solid-state supercapacitor using [I] electrodes at different bias voltages.

The Nyquist plots of a solid-state supercapacitor using the [I] electrodes at bias voltages of 0.8, 1.0 and 1.2 V are shown in Figure 5(b). The *ESR* was 5.8, 6.0 and 6.3 Ωcm^2, and R_{CT} was estimated at 4.6, 5.7 and 7.2 Ωcm^2 at bias voltages of 0.8, 1.0 and 1.2 V respectively. The dependence of resistance on potential again suggested that the charge/discharge process mainly took place at the electrode/electrolyte interface,[42,43] supporting the premise that engineering the interface between electrode and polymer electrolyte membrane could improve energy storage performance.

Four-point probe measurements of the electrodes without and with the interface layer gave similar electrical conductivities of 3.2 and 3.1 S cm^{-1} respectively, suggesting that adding the thin P-TiO_2 interface layer (1:10 thickness ratio of the interface layer to the electrode) had no significant effect on the overall in-plane electrical conductivity.

3.4 Capacitive performance and the effect of the interface layer

Figure 6(a) shows the cyclic voltammetry (CV) curves of the solid-state supercapacitors using the [N-TiO_2 + MWNT] electrodes without the interface layer (electrode [N]) and with the interface layer (electrode [I]) at a fast scan rate of 350 mV s^{-1}. The CV curve for the [I] electrodes showed a larger parallelogram area than the CV curve for the [N] electrodes, indicating faster charge/discharge kinetics after adding the interface layer.[44,45] Detailed capacitance estimation methods are shown in the SI. The specific capacitance per electrode estimated from the CV curves was 33.2 and 70.6 mF cm^{-2} (30.4 and 64.2 F g^{-1}) for the [N] and [I] electrodes respectively at 350 mV s^{-1}, where for the specific gravimetric capacitance estimation, the *total* mass of MWNTs, TiO_2 and ionomer was used.

Figure S2 in the SI shows the CV curves of the solid-state supercapacitor using [I] electrodes in different voltage windows at a faster scan rate of 400 mV s^{-1}. The CV curves maintained the parallelogram shape, indicative of facile ion transport.[14] The capacitance was estimated at 64.3 and 61.8 mF cm^{-2} per electrode at 1.3 and 1.4 V voltage windows respectively. However, current increased sharply at 1.3 V, which became more obvious at 1.4 V, indicative of possible irreversible reactions in this configuration.[38] Therefore, an operating voltage window of 1 V was used subse-

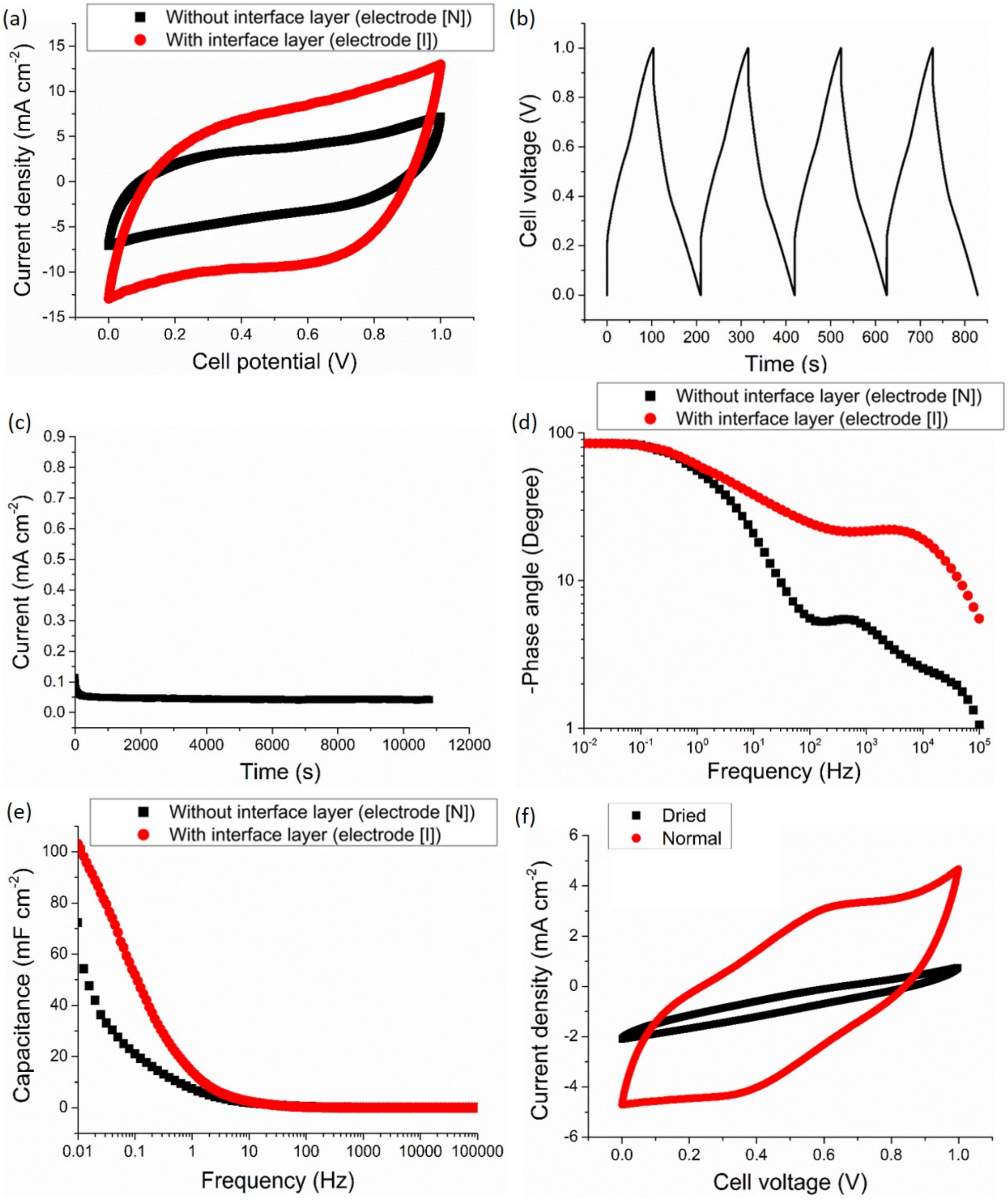

Figure 6: (a) CV curves of solid-state supercapacitors using [N-TiO$_2$ + MWNT] electrodes without ([N]) and with ([I]) an interface layer at a fast scan rate of 350 mV s^{-1}; (b) galvanostatic charge/discharge curves of the solid-state supercapacitor using [I] electrodes at 0.4 mA cm^{-2}; (c) current density of the corresponding supercapacitor at 1 V in relation to testing time; (d) impedance phase angle in relation to frequency for supercapacitors using [N] and [I] electrodes; (e) dynamic electrode capacitance per electrode from EIS in relation to frequency for the corresponding supercapacitors; and (f) CV curves of the supercapacitor using [I] electrodes at different hydration testing conditions at 350 mV s^{-1}: after drying in a vacuum oven at 105 ^{o}C for 3 hrs and then placing in air (normal humidity condition) for another 3 hrs.

quently.

Figures 6(b) and S3 in the SI show the galvanostatic charge/discharge curves of the solid-state supercapacitors using [N-TiO_2 + MWNT] electrodes without ([N]) and with ([I]) the interface layer at a slow charge and discharge rate of 0.4 mA cm^{-2} (0.36 A g^{-1}). Both figures show "sawtooth" shaped charge and discharge curves, which is characteristic of a supercapacitive behaviour (both EDLC and pseudo-capacitance).[44] The potential drop was reduced from 0.1 V for the [N] electrode to 0.07 V for the [I] electrode, which was lower than 0.08-0.2 V commonly reported for solid-state supercapacitors tested in similar conditions.[46,47] The specific capacitance per electrode estimated from the slope of the linear part of the discharge curve was 45.3 and 111.1 mF cm^{-2} (42.6 and 101.8 F g^{-1}) per electrode for the [N] and [I] electrodes respectively at 0.4 mA cm^{-2} (0.36 A g^{-1}). The areal capacitance was higher than 24.1 mF cm^{-2} per electrode previously reported at a similar charge/discharge rate for a TiO_2 nanotube array-only electrode using an aqueous Na_2SO_4 electrolyte.[48]

The coulombic efficiency of the [N] and [I] electrodes was 92% and 98% respectively (the detailed estimation method of coulombic efficiency is shown in the SI), again due to more facile ion transport across the [I] electrode/membrane interface. Figure S4 in the SI shows galvanostatic charge/discharge curves of the solid-state supercapacitor using [I] electrodes at a higher current of 0.8 mA cm^{-2} (0.73 A g^{-1}), where the shape of the curves was maintained, with a capacitance of 93.2 mF cm^{-2} (84.6 F g^{-1}) per electrode, a coulombic efficiency of 97% and a capacitance retention of 84% when the charge/discharge rate was doubled.

Given the effectiveness of the P-TiO_2 in the interface layer, the effect of the pore size in the P-TiO_2

was studied by reducing the templated pore diameter from ~25 nm to ~7 nm, shown in the SEM image in Figure S5. Figure S6 shows the galvanostatic charge/discharge curves of a solid-state supercapacitor again using [N-TiO_2 + MWNT] electrodes but now with an interface layer containing the P-TiO_2 with the reduced pore size, at the same charge/discharge rate of 0.4 mA cm^{-2}. The charge and discharge curves now deviated from the "sawtooth" shape shown in Figure 6(b); coulombic efficiency was reduced from 98 to 45%, and capacitance reduced by 68% to 36.1 mF cm^{-2}. The smaller P-TiO_2 pores were harder to fill with the ionomer essential to H^+ transport and may have also promoted irreversible ion trapping during charging. Thus, the importance of selecting both a TiO_2 morphology that wets the H_2SO_4 impregnated membrane and having an appropriate pore size that can be filled with ionomer was demonstrated.

Electrochemical stability measurements were performed in which the solid-state supercapacitor was first galvanostatically charged to 1 V at a current density of 1 mA cm^{-2}, and then the electrode current with time was monitored at the constant voltage of 1 V,[49,50] as shown in Figure 6(c). The current was very small at ~0.041 mA cm^{-2} and stable over 3 hrs, equivalent to 0.037 A g^{-1} and much less than 0.1 A g^{-1} that has been suggested to give acceptable stability.[50]

The dynamic capacitive performance of the solid-state supercapacitors using [N] and [I] electrodes was then assessed using electrochemical impedance spectroscopy (EIS). Figure 6(d) shows the impedance phase angle in relation to frequency for both types of electrode, with a reasonably flat response of $\sim$ -85^o at low frequency, conforming to near-capacitive behaviour.[39] At frequencies higher than 1.5 Hz, the [I] electrode maintained a significantly higher phase angle than the [N] electrode without the interface layer.

Electrode	**Electrolyte**	**Frequency (Hz) at a phase angle of -45^o**	**Phase angle (^{o}) at a frequency of 120 Hz**
[N-TiO$_2$ + MWNT] electrode ([N])	Polymer electrolyte Nafion membrane	2	-5.5
[N-TiO$_2$ + MWNT] electrode with a [P-TiO$_2$ + MWNT] interface layer ([I])	Polymer electrolyte Nafion membrane	5	-25

Table 4: A summary of frequency and phase angle achieved for the solid-state supercapacitor using [N-TiO$_2$ + MWNT] electrodes without ([N]) and with ([I]) the interface layer.

At a phase angle of -45^o, the [N] electrode in the solid-state supercapacitor configuration operated at $\sim$2 Hz, compared with $\sim$5 Hz for the [I] electrode; at 120 Hz, the [N] electrode had a phase angle of -5.5^o, compared with -25^o for the [I] electrode, as summarised in Table 4. Supercapacitors using carbon-based electrodes and liquid electrolytes have high frequencies and phase angles, e.g. a supercapacitor using vertically oriented graphene nanosheets electrodes and a KOH aqueous electrolyte exhibited a very high frequency of 15,000 Hz at -45^o, and a phase angle of -82^o at 120 Hz.[3] Although not always reported in detail, supercapacitors using polymer electrolyte membranes will always exhibit lower frequencies and phases angles,[51] e.g. the phase angle decreased sharply at -45^o and approached 0^o at high frequency.[13] Here, we show that although the frequency and phase angle of solid-state supercapacitors could not match those of liquid electrolyte-based supercapacitors, adding an interface layer between the electrode and polymer electrolyte membrane increased frequency by 2.5 times at -45^o and increased phase angle by 4.5 times at 120 Hz.

Figure 6(e) shows the dependence of dynamic capacitance per electrode measured from EIS in relation to frequency, following the procedures in[3,39,52]. Figure 6(e) shows that the [I] electrode with the interface layer exhibited a higher dynamic capacitance in the frequency range 0.01-120 Hz and Table 5 summarises the dynamic areal capacitances per electrode in the 0.01-120 Hz range. This

Electrode	**Specific areal capacitance (mF cm^{-2})**			
	0.01 Hz	0.1 Hz	10 Hz	120 Hz
[N-TiO_2 + MWNT] electrode ([N])	72.2	21.0	2.6	0.7
[N-TiO_2 + MWNT] electrode with a [P-TiO_2 + MWNT] interface layer ([I])	103.1	52.2	4.0	0.9

Table 5: A summary of the areal capacitance per electrode achieved for the solid-state supercapacitor using [N-TiO_2 + MWNT] electrodes with ([I]) and without ([N]) the interface layer.

frequency range is of particular technological interest because 0.12-70 Hz corresponds to the typical time constants of most high-power storage applications, such as cranking in a hybrid electric vehicle with an internal combustion engine, while 120 Hz corresponds to the typical time constant of high-frequency ripple filtering applications, which is dominated by the EDLC response.[53]

Overall, the performance of the solid-state supercapacitor after adding the interface layer was amongst the best-performing solid-state supercapacitors using similar electrode materials in the literature. For example, although a carbon quantum dot modified polypyrrole/titania electrode exhibited a high capacitance of 529 F g^{-1} in a liquid H_2SO_4 electrolyte, its capacitance dropped sharply to only 20 F g^{-1} at 5 mV s^{-1} in a solid-state supercapacitor configuration.[47] The high capacitance of the solid-state supercapacitor demonstrated here was due to the synergistic effects of: (i) a spraying and *in situ* drying process that allowed fabrication of porous electrodes consisting of an interconnected MWNT network with good electrical connectivity and an ionomer coating over all electrochemically active materials to facilitate ion conduction; (ii) an MWNT network that prevented excessive N-TiO_2 nanoparticle agglomeration so that both the MWNTs and N-TiO_2 nanoparticles provided a high surface area contributing to EDLC; and (iii) a thin P-TiO_2-based interface layer filled with ion-conducting ionomer contributed to improved wetting between the polymer membrane and the rest of the electrode, evidenced by faster ion transfer and a reduction in the electrode/polymer membrane interfacial ion transfer resistance.

Finally, we studied the performance of the solid-state supercapacitor with the interface layer under low and normal humidity conditions. Figure 6(f) shows a CV curve of the solid-state supercapacitor using [I] electrodes at 350 mV s^{-1}, after the whole supercapacitor was placed in a vacuum oven at 105 ^{o}C (within the stable Nafion and ionomer temperature range[54]) for 3 hrs. The CV curve shows a highly elongated and compressed parallelogram, indicating little charge storage, with an estimated capacitance of only 1.5 mF cm^{-2} per electrode at 350 mV s^{-1}. Figure 6(f) also shows the CV curve of the same dried solid-state supercapacitor after then leaving it in air for 3 hrs. The CV curve recovered a more parallelogram shape, indicating charge/discharge kinetics were partly restored, even after the preceding severe drying cycle, which is not usually applied for solid-state supercapacitors.[55] The estimated recovered capacitance was 13.3 mF cm^{-2} per electrode at 350 mV s^{-1}. Therefore, the capacitance increased by 9 times by simply leaving the supercapacitor in air without packaging even after severe drying, offering encouraging potential in, e.g. future wearable electronic applications.

Cyclic testing showed that the solid-state supercapacitor using the [I] electrodes with the interface layer retained 96% capacitance at a 1 mA cm^{-2} current density after 10,000 cycles.

4 Conclusions

A 450 nm porous TiO_2-based interface layer and then a 4.5 μm thick MWNT and non-porous TiO_2 nanoparticles-based electrode was sprayed on a polymer electrolyte membrane in a continuous process. In a solid-state supercapacitor configuration, this interface layer reduced interfacial resistance, enhanced ion transfer and improved dynamic capacitive performance. A capacitance of 111.1 mF cm^{-2} per electrode at 0.4 mA cm^{-2} after adding the interface layer was amongst the highest reported for solid-state supercapacitors. We have shown how engineering the membrane/electrode interface can transform solid-state supercapacitor performance and make best, conservative use of the relatively hard-to-obtain porous TiO_2. The general principle of interfacial engineering, exemplified here in a solid-state supercapacitor configuration, could find wider applicability in a variety of electrochemical energy storage and conversion devices.

Acknowledgments

The author would like to thank Prof Peter G. Bruce, Dr Andy Naylor and Mr Niccolo Guerrini for mercury porosimetry measurements and PECS sample preparation.

Associated content

Supporting Information. Detailed experimental, characterisation and capacitance estimation methods, cross-sectional SEM image of the electrode, SEM image of P-TiO_2 with smaller pores, CV curves at different voltage windows, galvanostatic charge/discharge curves of the electrode with and without the interface layer and with a smaller P-TiO_2 pore size at different charging rates.

References

[1] Beguin, F.; Frackowiak, E. *Supercapacitors - Materials, Systems, and Applications*, Wiley-VCH, 2013.

[2] Gao, P.-C.; Simon, P.; Favier, F. Silicon Carbide with Tunable Ordered Mesoporosity. *Microporous Mesoporous Mater.* **2013**, 180, 172-177.

[3] Miller, J. R.; Outlaw, R. A.; Holloway, B. C. Graphene Double-Layer Capacitor with AC Line-Filtering Performance. *Science* **2010**, 329, 1637-1639.

[4] Presser, V.; Heon, M.; Gogotsi, Y. Carbide-Derived Carbons - from Porous Networks to Nanotubes and Graphene. *Adv. Func. Mater.* **2011**, 21, 810-833.

[5] Beguin, F.; Presser, V.; Balducci, A.; Frackowiak, E. Carbons and Electrolytes for Advanced Supercapacitors. *Adv. Mater.* **2014**, 26, 2219-2251.

[6] Lufrano, F.; Staiti, P. Influence of the Surface-Chemistry of Modified Mesoporous Carbon on the Electrochemical Behavior of Solid-State Supercapacitors. *Energy Fuels* **2010**, 24, 3313-3320.

[7] Staiti, P.; Lufrano, F. Investigation of Polymer Electrolyte Hybrid Supercapacitor Based on Manganese Oxide-Carbon Electrodes. *Electrochim. Acta* **2010**, 55, 7436-7442.

[8] Delannoy, P.-E.; Riou, B.; Lestriez, B.; Guyomard, D.; Brousse, T.; Le Bideau, J. Toward Fast and Cost-Effective Ink-Jet Printing of Solid Electrolyte for Lithium Microbatteries. *J. Power Sources* **2015**, 274, 1085-1090.

[9] Choi, B. G.; Hong, J.; Hong, W. H.; Hammond, P. T.; Park, H. Facilitated Ion Transport in All-Solid-State Flexible Supercapacitors. *ACS Nano* **2011**, 5, 7205-7213.

[10] Anothumakkool, B.; Torris A. T.; Veeliyath, S.; Vijayakumar, V.; Badiger, M. V.; Kurungot, S. High-Performance Flexible Solid-State Supercapacitor with an Extended Nanoregime Interface through in situ Polymer Electrolyte Generation. *ACS Appl. Mater. Interfaces* **2016**, 8, 1233-1241.

[11] Brachet, M.; Brousse, T.; Le Bideau, J. All Solid-State Symmetrical Activated Carbon Electrochemical Double Layer Capacitors Designed with Ionogel Electrolyte. *ECS Electrochem. Lett.* **2014**, 3 (11), A112-A115.

[12] Soeda, K.; Yamagata, M.; Ishikawa, M. Outstanding Features of Alginate-Based Gel Electrolyte with Ionic Liquid for Electric Double Layer Capacitors. *J. Power Sources* **2015**, 280, 565-572.

[13] Ketabi, S.; Lian, K. The Effects of SiO_2 and TiO_2 Nanofillers on Structural and Electrochemical Properties of Poly(ethylene oxide)-$EMIHSO_4$ Electrolytes. *Electrochim. Acta* **2015**, 154, 404-412.

[14] Gao, H.; Lian, K. Proton-Conducting Polymer Electrolytes and Their Applications in Solid Supercapacitors: a Review. *RSC Adv.* **2014**, 4, 33091-33113.

[15] Prabhakaran, V.; Mehdi, B. L.; Ditto, J. J.; Engelhard, M. H.; Wang, B.; Gunaratne, K. D. D.; Johnston, D. C.; Browning, N. D.; Johnson, G. E.; Laskin, J. Rational Design of Efficient Electrode-Electrolyte Interfaces for Solid-State Energy Storage Using Ion Soft Landing. *Nat. Comm.* **2016**, 7:11399, DOI: 10.1038/ncomms11399.

[16] Yan, L.; Xu, Y.; Zhou, M.; Chen, G.; Deng, S.; Smirnov, S.; Luo, H.; Zou, G. Porous TiO_2 Conformal Coating on Carbon Nanotubes as Energy Storage Materials. *Electrochim. Acta* **2015**, 169, 73-81.

[17] Hyder, M. N.; Gallant, B. M.; Shah, N. J.; Shao-Horn, Y.; Hammond, P. T. Synthesis of Highly Stable Sub-8 nm TiO_2 Nanoparticles and Their Multilayer Electrodes of TiO_2/MWNT for Electrochemical Applications. *Nano Lett.* **2013**, 13, 4610-4619.

[18] Huang, C.; Young, N. P.; Grant, P. S. Spray Processing of TiO_2 Nanoparticle/Ionomer Coatings on Carbon Nanotube Scaffolds for Solid-State Supercapacitors. *J. Mater. Chem. A* **2014**, 2, 11022-11028.

[19] Huang, C.; Zhang, J.; Young, N. P.; Snaith, H. J.; Grant, P. S. Solid-State Supercapacitors with Rationally Designed Heterogeneous Electrodes Fabricated by Large Area Spray Processing for Wearable Energy Storage Applications. *Sci. Rep.* **2016**, 6:25684, DOI:10.1038/srep25684.

[20] Robinson, D. B. Optimization of Power and Energy Densities in Supercapacitors. *J. Power Sources* **2010**, 195, 3748-3756.

[21] Ebner, M.; Chung, D.-W.; Garcia, R. E.; Wood, V. Tortuosity Anisotropy in Lithium-Ion Battery Electrodes. *Adv. Energy Mater.* **2014**, 4, 1301278 1-6.

[22] Yamada, H.; Suzuki, K.; Nishio, K.; Takemoto, K.; Isomichi, G.; Moriguchi, I. Interfacial Phenomena between Lithium Ion Conductiors and Cathodes. *Solid State Ionics* **2014**, 262, 879-882.

[23] Weng, Y.-T.; Wu, N.-L. High-Performance Poly(3,4-ethylene-

dioxythiophene):Polystyrenesulfonate Conducting-Polymer Supercapacitor Containing Hetero-Dimensional Carbon Additives. *J. Power Sources* **2013**, 238, 69-73.

[24] Huang, C.; Grobert, N.; Watt, A. A. R.; Johnston, C.; Crossley, A.; Young, N. P.; Grant, P. S. Layer-by-Layer Spray Deposition and Unzipping of Single-Wall Carbon Nanotube-Based Thin Film Electrodes for Electrochemical Capacitors. *Carbon* **2013**, 61, 525-536.

[25] Huang, C.; Grant, P. S. One-Step Spray Processing of High Power All-Solid-State Supercapacitors. *Sci. Rep.* **2013**, 3:2393 DOI: 10.1038/srep02393.

[26] Zhao, Y.; Sun, J.; Chen, X.; Zhu, H.; Yang, W. Synthesis and High-Rate Performance of Spinel $Li_4Ti_5O_{12}$ with Core-Shell Hierarchical Macro-Mesoporous Structure. *New J. Chem.* **2014**, 38, 1173-1178.

[27] Vadiyar, M. M.; Bhise, S. C.; Patil, S. K.; Kolekar, S. S.; Shelke, A. R.; Deshpande, N. G.; Chang, J.-Y.; Ghule, K. S.; Ghule, A. V. Contact angle measurements: a preliminary diagnostic tool for evaluating the performance of $ZnFe_2O_4$ nano-flake based supercapacitors. *Chem. Commun.* **2016**, 52, 2557-2560.

[28] Javed, M. S.; Dai, S.; Wang, M.; Guo, D.; Chen, L.; Wang, X.; Hu, C.; Xi, Y. High Performance Solid State Flexible Supercapacitor Based on Molybdenum Sulfide Hierarchical Nanospheres. *J. Power Sources* **2015**, 285, 63-69.

[29] Sedlakova, V.; Sikula, J.; Majzner, J.; Sedlak, P.; Kuparowitz, T.; Buergler, B.; Vasina, P. Supercapacitor Equivalent Electrical Circuit Model Based on Charges Redistribution by Diffusion. *J. Power Sources* **2015**, 286, 58-65.

[30] Bisquert, J.; Garcia-Belmonte, G.; Bueno, P.; Longo, E.; Bulhoes, L. O. S. Impedance of

Constant Phase Element (CPE)-Blocked Diffusion in Film Electrodes. *J. Electroanal. Chem.* **1998**, 452, 229-234.

[31] Ho, C.; Raistrick, I. D.; Huggins, R. A. Application of A-C Techniques to the Study of Lithium Diffusion in Tungsten Trioxide Thin Films. *J. Electrochem. Soc.* **1980**, 127 (2), 343-350.

[32] Saha, D.; Li, Y.; Bi, Z.; Chen, J.; Keum, J. K.; Hensley, D. K.; Grappe, H. A.; Meyer, H. M. III; Dai, S.; Paranthaman, M. P.; Kaskar, A. K. Studies on Supercapacitor Electrode Material from Activated Lignin-Derived Mesoporous Carbon. *Langmuir* **2014**, 30, 900-910.

[33] Song, H.-K.; Hwang, H. Y.; Lee, K.-H.; Dao, L. H. The Effect of Pore Size Distribution on the Frequency Dispersion of Porous Electrodes. *Electrochim. Acta* **2000**, 45, 2241-2257.

[34] Z. Gao, Z. Cui, S. Zhu, Y. Liang, Z. Li, X. Yang, Design and Synthesis of MWNTs-TiO_2 Nanotube Hybrid Electrode and Its Supercapacitance Performance. *J. Power Sources* **2015**, 283, 397-407.

[35] Gao, H.; Virya, A.; Lian, K. Monovalent Silicotungstate Salt as Electrolytes for Electrochemical Supercapacitors. *Electrochim. Acta* **2014**, 138, 240-246.

[36] Xu, M.-W.; Zhao, D.-D.; Bao, S.-J. Mesoporous Amorphous MnO_2 as Electrode Material for Supercapacitor. *J. Solid State Electrochem.* **2007**, 11, 1101-1107.

[37] Beguin, F.; Frackowiak, E. *Carbons for Electrochemical Energy Storage and Conversion Systems*, CRC Press, 2010.

[38] Taberna, P. L.; Simon, P.;Fauvarque, J. F. Electrochemical Characteristics and Impedance Spectroscopy Studies of Carbon-Carbon Supercapacitors. *J. Electrochem. Soc.* **2003**, 150 (3), A292-A300.

[39] Cai, M.; Outlaw, R. A.; Butler, S. M.; Miller, J. R. A High Density of Vertically-Oriented Graphene for Use in Electric Double Layer Capacitors. *Carbon* **2012**, 50, 5481-5488.

[40] Cabanel, R.; Barral, G.; Diard, J. P.; Le Gorrec, B.; Montella, C. Determination of the Diffusion Coefficient of an Inserted Species by Impedance Spectroscopy: Application to the H/Hx Nb_2O_5 System. *J. Appl. Electrochem.* **1993**, 23, 93-97.

[41] Zhu, H.; He, H.; Xin, X.; Ma, X.; Zan, L.; Zhang, Y. Facile Synthesis of Li_2MnSiO_4/C/Graphene Composite with Superior High-Rate Performances as Cathode Materials for Li-Ion Batteries. *Electrochim. Acta* **2015**, 155, 116-124.

[42] Bard, A. J.; Faulkner, L. R. *Electrochemical Methods Fundamentals and Applications*, Wiley, 2001.

[43] O'Neill, L.; Johnston, C.; Grant, P. S. Enhancing the Supercapacitor Behaviour of Fe_3O_4/FeOOH Coaxial Nanowire-Carbon Nanotube Hybrid Electrodes in Aqueous Electrolytes. *J. Power Sources* **2015**, 274, 907-915.

[44] Goubard-Bretesche, N.; Crosnier, O.; Payne, C.; Favier, F.; Brousse, T. Nanocrystalline $FeWO_4$ as a Pseudocapacitive Electrode Material for High Volumetric Energy Density Supercapacitors Operated in an Aqueous Electrolyte. *Electrochem. Commun.* **2015**, 57, 61-64.

[45] Grancisco, B. E.; Jones, C. M.; Lee, S.; Stoldt, C. R. Nanostructured All-Solid-State Supercapacitor Based on Li_2S-P_2S_5 Glass-Ceramic Electrolyte. *Appl. Phys. Lett.* **2012**, 100, 103902.

[46] Chen, Y.-R.; Chiu, K.-F.; Lin, H. C.; Chen, C.-L.; Hsieh, C. Y.; Tsai, C. B.; Chu, B. T. T. Graphene/Activated Carbon Supercapacitors with Sulfonated-Polyetheretherketone as Solid-State Electrolyte and Multifunctional Binder. *Solid State Sci.* **2014**, 37, 80-85.

[47] Xie, Y.; Du, H. Electrochemical Capacitance of a Carbon Quantum Dots-Polypyrrole/Titania Nanotube Hybrid. *RSC Adv.* **2015**, 5, 89689-89697.

[48] Li, Z.; Ding, Y,; Kang, W.; Li, C.; Lin, D.; Wang, X.; Chen, Z.; Wu, M.; Pan, D. Reduction Mechanism and Capacitive Properties of Highly Electrochemically Reduced TiO_2 Nanotube Arrays. *Electrochim. Acta* **2015**, 161, 40-47.

[49] Soavi, F.; Arbizzani, C. Leakage Current and Self-Discharge of Ionic Liquid-Based Supercapacitors. *J. Appl. Electrochem.* **2014**, 44, 491-496.

[50] Lukatskaya, M. R.; Bak, S.-M.; Yu, X.; Yang, X.-Q.; Barsoum, M. W.; Gogotsi, Y. Probing the Mechanism of High Capacitance in 2D Titanium Carbide Using in situ X-ray Absorption Spectroscopy. *Adv. Energy Mater.* **2015**, 5, 1500589 1-4.

[51] Hastak, R. S.; Sivaraman, P.; Potphode, D. D.; Shashidhara, K.; Samui, A. B. High Temperature All Solid State Supercapacitor Based on Multi-Walled Carbon Nanotubes and Poly[2,5 benzimidazole]. *J. Solid State Electrochem.* **2012**, 16, 3215-3226.

[52] Lufrano, F.; Staiti, P. Performance Improvement of Nafion Based Solid-State Electrochemical Supercapacitor. *Electrochim. Acta* **2004**, 49, 2683-2689.

[53] Miller, J. R.; Outlaw, R. A.; Holloway, B. C. Graphene Electric Double Layer Capacitor with Ultra-High-Power Performance. *Electrochim. Acta* **2011**, 56, 10443-10449.

[54] Chalkova, E.; Pague, M. B.; Fedkin, M. V.; Wesolowski, D. J.; Lvov, S. N. Nafion/TiO_2 Proton Conductive Composite Membranes for PEMFCs Operating at Elevated Temperature and Reduced Relative Humidity. *J. Electrochem. Soc.* **2005**, 152 (6), A1035-A1040.

[55] Li, Y.; Mei, Y.; Zhang, L.-Q.; Wang, J.-H.; Liu, A.-R.; Zhang, Y.-J.; Liu, S.-Q. Manganese

Oxide Nanowires Wrapped with Nitrogen Doped Carbon Layer for High Performance Supercapacitors. *J. Colloid Interface Sci.* **2015**, 455, 188-193.

Table of contents/abstract graphic